



HAL
open science

Facile One-Pot Synthesis of White Emitting Gold Nanocluster solutions composed of Red, Green and Blue Emitters

Laureen Moreaud, Janak Prasad, Serge Mazeres, Cécile Garcia-Marcelot, Clothilde Zerbino, Rodolphe Antoine, Olivier Heintz, Erik Dujardin

► **To cite this version:**

Laureen Moreaud, Janak Prasad, Serge Mazeres, Cécile Garcia-Marcelot, Clothilde Zerbino, et al.. Facile One-Pot Synthesis of White Emitting Gold Nanocluster solutions composed of Red, Green and Blue Emitters. *Journal of Materials Chemistry C*, 2022, 10 (6), pp.2263-2270. 10.1039/D1TC04874K . hal-03526200

HAL Id: hal-03526200

<https://hal.science/hal-03526200>

Submitted on 14 Jan 2022

HAL is a multi-disciplinary open access archive for the deposit and dissemination of scientific research documents, whether they are published or not. The documents may come from teaching and research institutions in France or abroad, or from public or private research centers.

L'archive ouverte pluridisciplinaire **HAL**, est destinée au dépôt et à la diffusion de documents scientifiques de niveau recherche, publiés ou non, émanant des établissements d'enseignement et de recherche français ou étrangers, des laboratoires publics ou privés.

Facile One-Pot Synthesis of White Emitting Gold Nanocluster solutions composed of Red, Green and Blue Emitters

Laureen Moreaud,^a Janak Prasad,^a Serges Mazères,^b Cécile Marcelot,^a Clothilde Comby-Zerbino,^c Rodolphe Antoine,^c Olivier Heintz^d and Erik Dujardin^{*a}

Gold nanoclusters (AuNC) have emerged as a new class of stable and biocompatible photo-emitters. While red emitting clusters comprising ca. 20-25 Au atoms are readily synthesized by several methods, smaller clusters with higher energy luminescence are much less commonly reported. Here, we report on a straightforward one-step synthesis of red, green, blue and violet emitting AuNC in mild conditions. Produced in pure ethylene glycol, the structural and optical properties of the AuNC are tuned by adding either aniline or indole. By combining high-resolution TEM, electrospray ionization mass spectrometry, X-ray photoelectron and photoluminescence spectroscopy, we identify Au₆ (blue), Au₁₁ (green) and Au₂₂ (red) in solutions produced with aniline. This tricolor mixture produces a pure white luminescence under broadband excitation. The Au₅ (violet) and Au₇ (blue) produced with indole exhibit a large 27% quantum yield making them among the brightest blue emitting gold clusters. Importantly, when the AuNC are capped with a thiopegylated ligand shell bearing a terminal carboxylate, amine or biotin, they are made water soluble and stable while preserving intact their photo-physical characteristics. This work provides an easy access to robust emitters with tunable fluorescence and surface functionality for potential use in biolabelling, hyperspectral sensing or display technology.

Introduction

Luminescent materials have a tremendous potential for applications as bio-labeling^{1,2}, metal ion sensing³, catalytic reactions⁴ and light-emitting displays.⁵ Within the extended family of emitters, the gold nanoclusters (AuNCs) have recently appear as excellent substitutes to semiconductor quantum dots thanks to a much lower *in vivo* cytotoxicity, smaller size and easier surface passivation^{6–8} but also to molecular dyes owing to a much higher photostability and larger Stokes shifts.⁹ The emission properties of AuNC arise from the confinement of the conduction electrons when the cluster size reaches below the de Broglie length (~ 1 nm).¹⁰ These chromophores are distinct from metal ion complexes which may also luminesce due to metal-ligand charge transfer.¹¹ In solution,^{12,13} AuNC were first synthesized by template-assisted synthesis inside proteins or dendrimers cavities,^{14–16} by chemical core etching of bigger nanoparticles^{17,18} or by reduction of Au(III) ions in the presence of stabilizing agents.^{3,19,20} These protocols almost systematically lead to red-emitting AuNCs with few recent reports of blue and green emitters.^{20–22} Importantly, AuNCs generally suffer from lower quantum yields (QY) compared to molecular dyes molecules, especially green-emitting AuNCs, the QY of which hardly reaches 5%.^{19–21} Among the several approaches

developed to overcome this limitation,²³ the most efficient one consists in modifying the ligands on the surface of the gold clusters. For example, PAMAM dendrimers matrix^{15,16} and rigidified ligand shell with tetraoctylammonium (TOA) cations of Au(I)-thiolate clusters^{22,24} have been reported.

Herein, we report a facile one-pot synthesis of stable gold AuNCs by the reduction, with aniline, of HAu(III)Cl₄ in ethylene glycol (EG) leading to mixtures of red, green and blue emitters with repeatable composition and producing a pure white luminescence. When replacing aniline with indole, we obtain only higher energy violet and blue emitters. We report on extensive structural and photophysical characterizations of the AuNCs that exhibit quantum yields up to 30%. Importantly, we successfully stabilize the same AuNCs in water by functionalizing their surface with short cationic or anionic ligands as well as with a longer biotinylated ligand suitable for biomarking and imaging applications.

Results and discussion

Gold clusters are synthesized by mixing a 10 mM gold(III) chloride aqueous solution with pure EG at 55°C for 20 min, followed by the addition of 100 mM aniline in EG and further stirring for 5 min (See details in Experimental Section). Then, the solution is kept unstirred at 55°C for 24 h. A variation of this protocol consists in replacing aniline with indole in the exact same conditions. In both cases, an orange solution of AuNC is obtained with a final concentration of about 20 μ M. Several control experiments described in Section 1 of the electronic supporting information (ESI) demonstrate that the fluorescence is observed only when AuNC are present and cannot be ascribed to aniline, indole, EG or their by-products. In the absence of other capping agents, the excess EG ensures the AuNC stability and prevents aggregations into bigger, non-fluorescent

^a CEMES, CNRS UPR 8011 – Université Toulouse III P. Sabatier, 29 rue J. Marvig, 31055 Toulouse, France. Email: dujardin@cemes.fr

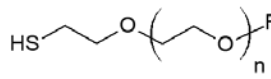
^b IPBS, CNRS UMR 5089 – Université Toulouse III P. Sabatier, 205 route de Narbonne, 31077 Toulouse, France.

^c ILM, CNRS UMR 5306 – Université C. Bernard Lyon 1, 69100 Villeurbanne, France.

^d ICB, CNRS UMR 6303 – Université de Bourgogne Franche-Comté, 9 rue A. Savary, 21078 Dijon, France

Electronic Supplementary Information (ESI) available: Fluorescence control experiments; UV-visible absorption spectra; repeatability tests; 2D fluorescence maps of thiopegylated samples; Jellium model calculations; XPS data; ESI-MS data; HRTEM and AFM data and analysis; Quantum yield analysis.

particles (ESI Fig. S1). Yet, in anticipation of biolabeling or biosensing applications, as-synthesized AuNC have been transferred into water with long-term stability by covalent surface functionalization, as detailed in the Experimental Section, with HS-PEG_n-R ligands (Table 1). Short ($n = 12$) ligands with amine ($R = (\text{CH}_2)_2\text{-NH}_2$) or carboxylate ($R = \text{CO}_2\text{H}$) head groups and long ($n \sim 70$) ligands with amine ($R = (\text{CH}_2)_2\text{-NH}_2$) or biotin ($R = \text{CO}-(\text{CH}_2)_4\text{-biotin}$) head groups have been considered.



| | n | R |
|-------------------|----------|--|
| (1a), (1i) | 12 | $-(\text{CH}_2)_2\text{-NH}_2$ |
| (2a), (2i) | 12 | $-\text{CO}_2\text{H}$ |
| (3a), (3i) | 70 | $-(\text{CH}_2)_2\text{-NH}_2$ |
| (4a), (4i) | 70 | $-\text{CO}-(\text{CH}_2)_4\text{-biotin}$ |

Table 1. Structure of the thiopegylated ligands used for the AuNC functionalization. The indexes a and i denote whether the reducing agent used was aniline or indole respectively.

As-synthesized solutions present a small localized plasmon resonance in the UV-visible absorption spectrum that disappears after functionalization (ESI Fig. S2). This suggests that plasmonic nanoparticles with sizes exceeding 3 nm are effectively eliminated by the centrifugation, surface thiopegylation and solvent transfer steps. Interestingly, all AuNCs solutions produce a strong broadband fluorescence, the detailed spectral features of which are slightly different if aniline or indole is used in the initial synthesis. Figure 1 shows spectra and 2D maps of the fluorescence intensity as a function of the emission (λ_{em}) and excitation (λ_{ex}) wavelengths for the centrifuged, but non-functionalized, aniline (Figs. 1a,b) and indole (Figs. 1c,d) AuNCs in EG. In the 2D maps, high intensity patches are clearly visible that can be associated with classes of emitters. For aniline AuNCs, the predominant feature of Figure 1a is the strong green emission centered at $\lambda_{\text{em}} = 500$ nm and $\lambda_{\text{ex}} = 425$ nm. Green-emitting AuNCs are uncommon^{25,26} but emission at $\lambda_{\text{em}} = 510$ nm has been reported for dendrimer-stabilized Au₁₃.¹⁶ Two other distinct patches reveal red emission at $\lambda_{\text{em}} = 640$ nm and $\lambda_{\text{ex}} = 510$ nm and blue emission at $\lambda_{\text{em}} = 425$ nm and $\lambda_{\text{ex}} = 310$ nm. The former are reminiscent to the classical red fluorescence of BSA-stabilized Au₂₅ ($\lambda_{\text{em}} = 640$ nm)¹⁴ and lysine-capped Au₂₅ ($\lambda_{\text{em}} = 657$ nm).²⁷ The latter are even rarer except for the report of dendrimer-embedded Au₈ emitting at $\lambda_{\text{em}} = 456$ nm.¹⁶ An extra contribution from a violet emission with very low intensity

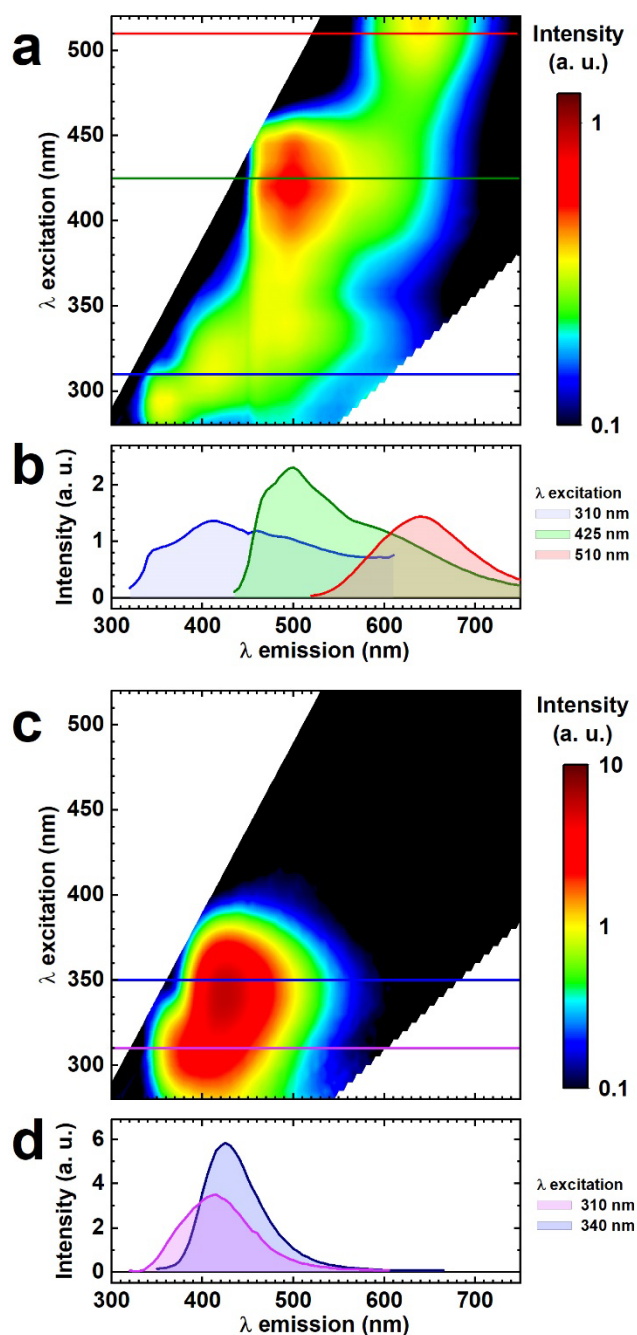


Figure 1. (a) 2D plot and (b) representative spectra of the fluorescence intensity at room temperature of aniline AuNC as a function of emission, λ_{em} , and excitation, λ_{ex} , wavelengths. (c) 2D plot and (d) representative spectra of indole AuNC fluorescence intensity. Colored line traces in (a) and (c) correspond to the spectra in (b) and (d) respectively.

($\lambda_{\text{em}} = 360$ nm and $\lambda_{\text{ex}} = 290$ nm) may also be observed in most samples. Indole AuNCs display a much more restricted, yet more intense, emission pattern at shorter wavelengths (Fig. 1c). The fluorescence is mainly observed at $\lambda_{\text{em}} = 425$ nm and $\lambda_{\text{ex}} = 350$ nm with a clear secondary adjacent patch of violet emission at $\lambda_{\text{em}} = 400$ nm and $\lambda_{\text{ex}} = 310$ nm. Such a high energy luminescence has only been observed for very small, dendrimer-embedded Au₅ nano-clusters with $\lambda_{\text{em}} = 386$ nm.¹⁶ These emission features are highly reproducible for all our synthesis batches with a moderate variation of relative

fluorescence intensities which suggests a consistent set of AuNC structures for indole or aniline protocols with a varying relative abundance of each AuNC type (ESI Figs. S3, S4).

The excitation/emission characteristics of AuNCs depend on the size of their Au cores, on the nature of the ligands and on the Au-ligand bond structure. The size evolution of the emission wavelength of AuNCs comprising more than 20 atoms is well described by the power law of the jellium model, $\lambda_{em} = E_f \cdot n^{-1/3}$, with $E_f = 5.46$ eV.¹⁶ For small ($n < 20$) AuNCs stabilized with thiolated ligands, L, a pure Au_n core with a ligand shell^{28,29} or an oligomeric Au_nL_n chains³⁰ have been observed for which the jellium model is not valid in principle. In this case, TD-DFT calculations are usually applied, when the precise AuNC structure is known.^{31,32} Yet, the simple jellium model has been shown to remain empirically predictive down to $n = 3$.^{16,33} We qualitatively estimate the Au_n cluster size from the jellium model applied to the main emission wavelengths found in Figs. 1a and 1c. Conservatively taking into account the spread of the emission features, we find $n = 5 \pm 1$ and $n = 7 \pm 1$ for indole AuNCs and $n = 6 \pm 2$, $n = 11 \pm 2$ and $n = 22 \pm 4$ for aniline AuNCs (ESI Table S5). Our simple one-step protocol consistently leads to mixtures of a small number of different AuNC with reproducible fluorescence signature.

In order to gain better insight into the AuNC structure, electrospray ionization mass spectrometry (ESI-MS) and X-ray photoelectron spectroscopy (XPS) analysis were performed. Water-soluble clusters were produced by functionalization with thiopegylated ligands bearing a charged headgroup (amine, carboxylate or biotin) as summarized in Table 1. The length of the PEG spacer was chosen either long (70 EG monomers, AuNC 3i,a and 4i,a), to favour long-term colloidal stability or short (12 EG monomers, AuNC 1i,a and 2i,a) to maximize the relative contribution of the Au core to the ESI-MS signal. Interestingly, in contrast to earlier reports that suggested an increase of the core size from Au₁₁ to Au₂₅ during ligand exchange,³⁴ the thiopegylation of both indole and aniline AuNC and their transfer into water did not affect the number nor the spectral positions (λ_{em} ; λ_{ex}) of the fluorescence 2D patterns (ESI, Fig. S4). The only change is a variation of the relative intensities of each feature for the aniline AuNC upon capping with short ligands, and particularly a reduction of the red and green emissions in favour of the blue and violet ones. This is ascribed to a reduction in abundance of red and green emitters by the oxidative etching of the thiolated molecules¹². Remarkably indole AuNC show absolutely no spectral or intensity change upon thiopegylation (ESI, Fig. S4). XPS analysis of functionalized AuNCs confirms the presence of the ligands and gold core (ESI, Fig. S6). The absence of nitrogen signal (399 eV) in the case of carboxylated ligands suggests that the reducing agents (aniline or indole) do not persist on the AuNC surface after thiopegylation. Conversely, it is present in AuNC bearing both amine and biotin terminated ligands. The S2p (163 and 168 eV) and the C1s (285 and 286 eV) peaks from the thioPEG linker are equally observed on all AuNCs. The Au4f (80-90 eV) peaks provide direct information on the gold core (Fig. 2). The curve fitting reveals a consistent shift between the two pairs of 4f7/2 and 4f5/2 peaks that varies from 0.65 to 0.85 eV for the different types of AuNC. This shift

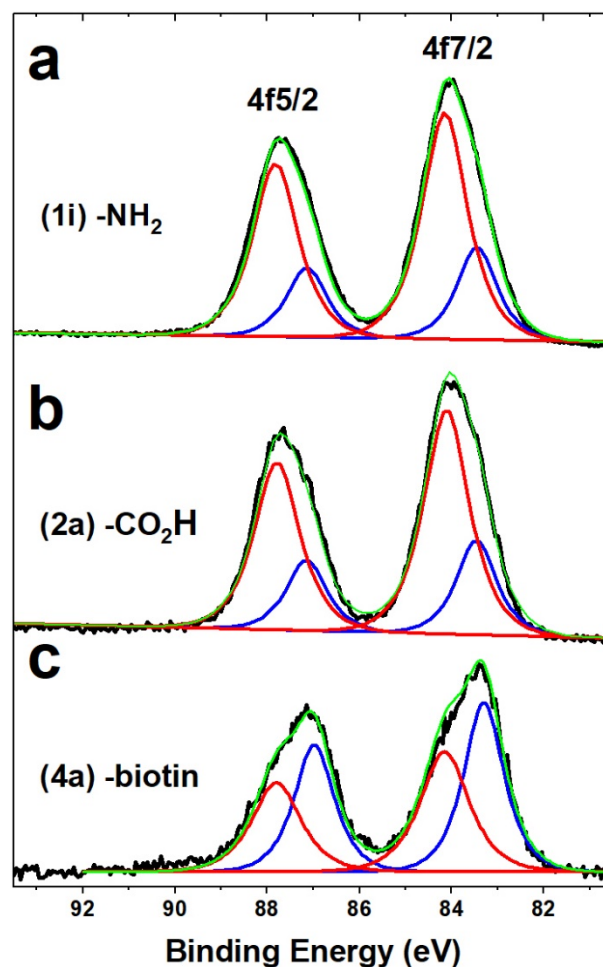


Figure 2. Au 4f XPS spectra of thiopegylated AuNC with (a) $-\text{PEG}_{12}-(\text{CH}_2)_2-\text{NH}_2$ (1i), (b) $-\text{PEG}_{12}-\text{CO}_2\text{H}$ (2a) and (c) $-\text{PEG}_{70}-\text{CO}-(\text{CH}_2)_4-\text{biotin}$ (4a). The 4f7/2 and 4f5/2 peaks are decomposed into two contributions coming from neutral (blue) and charged (red) Au atoms. The overall fits are shown in green.

is attributed to a charge effect that can be used to estimate the ratio of partially coordinated and charged peripheral gold atoms to quasi neutral, highly coordinated core atoms. This ratio is 2.40 ± 0.04 for AuNC 2a and 1i but only 0.70 for AuNC 4a and could indicate the coexistence of 2D and 3D Au_n core structures.^{28,29}

ESI-MS operated in negative mode provides the mass-to-charge (m/z) spectrum of Au_n(S-PEG₁₂-CO₂H)_p clusters 2a shown in Figure 3a that reveals the presence of Au₇(S-PEG₁₂-CO₂H)₇₋₈ and Au₁₀(S-PEG₁₂-CO₂H)₁₀ clusters (peaks (1)-(2) and (3) respectively) (details in ESI Section 7).³⁵ Peaks labelled (i)-(iii) originate from ligand oligomers therefore unidentified PEG fragments could arguably account for the unlabelled peaks in the $m/z = 1900-2300$ region. Figure 3b displays the spectrum of sample 2i, where Au₁₀(S-PEG₁₂-CO₂H)₁₀, Au₁₁(S-PEG₁₂-CO₂H)₁₁ and Au₁₂(S-PEG₁₂-CO₂H)₁₂₋₁₄ are identified (details in ESI Section 7). When the terminal carboxylic group in 2a,i is replaced by the amino moiety in 1a,i, positive mode ESI-MS spectra show multi-peak distributions of charge states for which the mass ranges between ~ 6.4 to ~ 17 kDa (ESI, Fig. S7). Interestingly, in 1a, species with larger masses up to 16 500 Da are observed, which indicates the presence of larger AuNCs up to Au₂₅(S-PEG₁₂-

NH₂)₁₉. The coexistence of smaller ($4 \leq n \leq 7$) and intermediate sized ($10 \leq n \leq 12$) AuNCs in both aniline and indole carboxylated samples suggests that a more effective oxidative etching might take place during ligand binding with carboxylated PEG ligands compared to the amino counterparts.^{12,21}

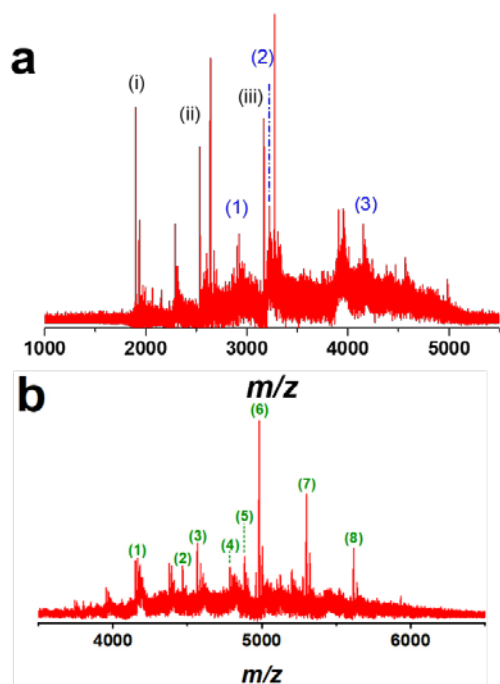


Figure 3. Negative mode mass-to-charge ESI-MS spectra for (2a) and (2i) AuNCs respectively exchanged with HS-PEG₁₂-COOH from (a) aniline and (b) indole gold clusters. Peaks (i) to (iii) are attributed to ligand oligomers. See main text and ESI Section 7 for details.

The biotinylated AuNC 4a/4i were functionalized with a high molecular weight PEG₇₀ spacer in order to ensure their long term stability in aqueous solution. Their *m/z* spectra in positive mode ESI-MS show a broad distribution of charge states spanning from *m/z* 1700 to 3500 (ESI Fig. S8) that can be deconvoluted with a multiplicative correlation algorithm.^{36,37} In Figure S8b, the estimated AuNC mass distribution reveals two peaks in the 20 000-27 000 Da range that may be assigned to Au₆(S-PEG₇₀-Biotin)₆ and Au₇(S-PEG₇₀-Biotin)₇ cluster compositions. The large mass of the PEG₇₀ ligand molecules (~ 3400 Da) with respect to the estimated Au core (ca. 1200-2000 Da) prevents a more precise assignment to a specific Au cluster size and the presence of higher size, up to Au₁₀(S-PEG₇₀-Biotin)₁₀, or fragments of larger clusters cannot be ruled out. Direct structural characterization of AuNC is challenging, for example, high resolution transmission electron microscopy (HRTEM) can hardly determine the structure of AuNC smaller than 1 nm. HRTEM performed on our as-synthesized, non-thiolated AuNCs shows no sign of aggregation. A lognormal size distribution, which certainly underestimates the amount of sub-nm AuNC, is observed with a global mean of 2.9 and 2.4 nm for

aniline and indole-reduced clusters respectively (ESI, Fig. S9). About 30-35% of the observed clusters have sizes below 2 nm with penta-twinned, single-twinned and single crystalline structures. The latter show smaller oblong morphology and account for one third of the sub-2 nm observable objects. In spite of a very faint contrast, longer and smaller axes of 1.51 ± 0.35 nm (resp. 1.90 ± 0.47 nm) and 1.07 ± 0.11 nm (resp. 1.04 ± 0.16 nm) can be determined for aniline (resp. indole) samples (ESI, Fig. S10d). These observations are consistent with Au clusters comprising 20-25 atoms and less, which may adopt stable 2D oblong morphologies.^{28,29}

Fluorescence lifetime measurements were carried out on as-synthesized indole AuNC (Fig. 4, blue). The fluorescence decay follows a single exponential trend with a lifetime of 8 ns. Since the excitation wavelength is 380 nm, this time constant is associated to the larger AuNC ($n = 7 \pm 1$) only. However, the fit to the fluorescence decay of aniline AuNC (Fig. 4, red) requires two distinct time constants of 5 ns and 90 ns with a relative abundance of 90% and 10% respectively, which are associated to the green ($n = 11 \pm 2$) and red ($n = 22 \pm 4$) emitting clusters. Interestingly, similar measurements performed on thiopegylated samples yielded exactly identical decay curves and fitting lifetimes (ESI, Fig. S12), which corroborates the fact that the functionalization procedure does not affect significantly the electronic structure and photophysics of our AuNC. These values match the reported 5-10 ns decay rates associated with sub-15 atom green-emitting AuNC and the 30-150 ns lifetimes of red and near-IR AuNC emitters comprising more than 20 atoms.^{21-23,38} The latter longer lifetime is also consistent with the ESI-MS observations that larger AuNC comprise more ligands able to better stabilize the excited state. The emitter brightness is quantified by measuring the quantum yield (QY) as detailed in the Experimental Section. The QY of the blue and green aniline AuNC is 5% and it is about 1% for the red clusters, close to the usual values reported in the literature for similar sizes.^{14,20,22} The QY of violet and blue indole AuNCs reach as high as $27.4\% \pm 2.5\%$ that is only matched by AuNC encapsulated within a thick and rigid shell such as PAMAM, cellulose or large PEG_n ($n > 550$) ligand (ESI Fig. S13).^{15,16} The QY of our clusters varies very marginally upon thiopegylation and transfer into water (ESI Table S14), which once again suggests that the HS-PEG_n-R ligand introduction does not affect the structure nor the immediate environment of the emitting centers.

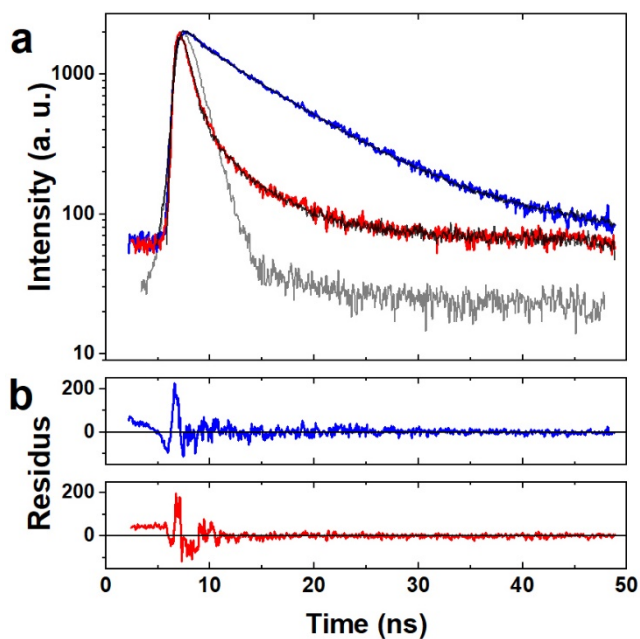


Figure 4. (a) Fluorescence lifetime measurements and (b) fit residues of aniline (red) and indole (blue) AuNCs. In (a), fits are in black and the POPOP reference is in grey.

The as-prepared solution of aniline AuNCs consistently comprises red, blue and green emitters, with their relative abundance only slightly varying (ESI, Fig. S3). The spectra in Figure 1b taken at three representative excitation wavelengths show a rather uniform emission over the entire visible range. The combination of red, green and blue emitters is classically used in LEDs to create white light with warmer or cooler hues³⁹ resulting from the difference in spectral width of the three components.^{40,41,42} A similar emission can be obtained from perylene-coated AuNC.⁴³ A broadband excitation of our emitter system is simulated by summing up the emission spectra of Figure 1a for $400 \leq \lambda_{\text{ex}} \leq 700$ nm as shown in Figure 5 inset (blue). The CIE XY map coordinates are thus calculated for each AuNC synthesis and reported on the 1931 CIE map in Figure 5. The CIE coordinates from aniline AuNC spectra are all gathered near the center of the map corresponding to a white emission. This white emission is experimentally recorded from 400 to 700 nm upon excitation with a Hg lamp through a 350 to 500 nm bandpass filter (See Experimental Section for details). The black spectrum in Figure 5 inset is very similar to the numerically cumulated spectrum. The small discrepancies below 350 nm and above 650 nm are attributed to the filter performances in the cut-off regions. The CIE coordinates of the experimental luminescence spectrum with broadband excitation also fall close to the central white spot, thus validating the methodology based on processing the 2D maps and confirming the white emission of the solutions of aniline AuNCs. Similarly, the CIE coordinates of indole AuNC solutions are located in the blue corner, as expected. Thiopegylation and transfer into water have no effect on the emission color of the functionalized indole AuNC solutions. A moderate shift away from pure white emission towards the blue hues is observed for the functionalized aniline AuNC solutions, which is consistent with

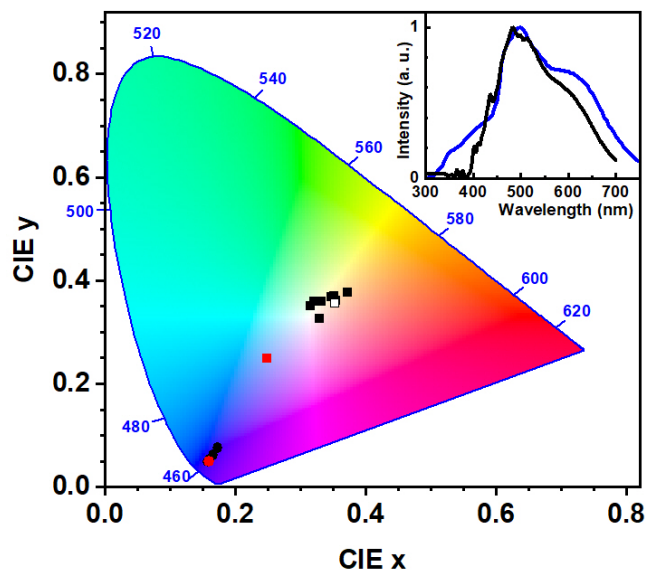


Figure 5. Trichromatic coordinates of aniline (square) and indole (circle) AuNC solutions on the CIE 1931 color space before (black) and after (red) thiopegylation. The white square corresponds to the emission of the aniline AuNC upon broadband excitation (black spectrum in inset). Inset: Normalized white emission spectra of aniline AuNC obtained by 350-500 nm broadband excitation (black) or by summation of all spectra for $400 \leq \lambda_{\text{ex}} \leq 700$ nm in Fig. 3a (blue).

the reduction of the relative abundance of red emitters after ligand binding.

Conclusions

As a conclusion, we have presented here a facile one-pot synthesis of white or bright blue emitting AuNC solutions in EG and their non-invasive functionalization with hydrophilic ligands that preserves their luminescent characteristics. By combining structural and photophysical methods, we have identified a mixture of blue (Au_n , $n = 6 \pm 2$), green (Au_n , $n = 11 \pm 2$) and red (Au_n , $n = 22 \pm 4$) AuNC consistently produced with aniline. This unique tricolor mixture produces a quite pure white luminescence that can be activated by a 350-500 nm broadband excitation. When replacing aniline with indole, no red emitter is obtained and the mixture only comprises violet (Au_n , $n = 5 \pm 1$) and blue (Au_n , $n = 7 \pm 1$) AuNC that exhibit a very high QY making them among the brightest blue emitting gold clusters. All AuNC could be functionalized with thioPEG ligands bearing carboxylate, amine or biotin terminal groups and stabilized in water by adjusting the PEG length though keeping it 10 to 60 times shorter than previous reports.³⁸ No significant changes of their optical properties was observed upon functionalization and the sizes of thiopegylated AuNCs measured by ESI-MS confirmed the ones derived from the photophysical responses. Our direct and robust synthesis of biocompatible, non-bleaching emitters with broadband luminescence beyond the standard red-emitting Au25 clusters offers promising solutions for emerging hyperspectral bio-labeling and sensing applications.^{12,44,45}

Experimental

Synthesis and Functionalization of Au clusters (AuNCs). All chemicals have been purchased from Sigma-Aldrich except tetrachloroaurate(III) ($\text{HAuCl}_4 \cdot 3\text{H}_2\text{O}$, Alpha Aesar) and where mentioned otherwise. 0.18 mL of a 10 mM HAuCl_4 aqueous solution and 1 μL of 1.0 M HCl are mixed in 1.82 mL of ethylene glycol (99.8%) and heated at 55°C for 20 min upon stirring. 5 μL of 0.1 M aniline 99.5% (or indole >99%) in ethylene glycol (EG) are added, the solution is stirred for another 5 min and then stored at 55°C for 24 h. Control experiments of this protocol performed in the absence of aniline (or indole), of EG or of HAuCl_4 have been conducted and are described in SI section 1. Water-stable AuNCs solutions are obtained from the AuNCs in EG by functionalizing their surface with thiopegylated HS-PEG_n-R ligands described in Table 1 and following the same protocol. The as-synthesized AuNC solution in EG is dialyzed against deionized water for 4 hours to remove excess EG with a 500-1000 Da MWCO Float-A-Lyzer (Spectrum Labs) membrane. The final volume of the dialyzed aqueous solution is 4 mL. 50 μL of a 10 mg.mL⁻¹ solution of HS-PEG_n-R is added to 2 mL of the dialyzed solution and left overnight at room temperature to allow covalent binding of the Au surface by the thiols. A second dialysis identical to the first one is performed to remove all unbound HS-PEG_n-R.

Structural characterization. High-Resolution Transmission Electron Microscopy (HRTEM) is performed on a Cs corrected Hitachi HF3300 microscope (I2TEM) operated at 300 kV with a Gatan Digital Micrograph interface. A 10 μL drop of AuNC solution is deposited on a carbon-coated copper grid, wicked off after 10 min then the grid is dried and rinsed once with DI water. Electrospray ionization mass spectroscopy (ESI-MS) is performed on a Bruker-Daltonics micro-qTOF quadrupole time-of-flight spectrometer with mass resolution ~10 000. The samples are prepared by ultrafiltration (5kDa) and dilution of the mother solution to a final concentration of 1 mg/mL in water. The samples are analyzed in both positive and negative ion modes. Each data point accumulates spectra over 5 min. The deconvolution is performed with a multiplicative correlation algorithm (MCA)^{46,47} for a distribution of positives charges between 7 and 11. External calibration is carried out with a set of synthetic peptides. Chemical surface analyses of the samples were carried out by XPS on a Versaprobe 5000 spectrometer (ULVAC-PHI apparatus), equipped with a monochromated and focalized Al K α X-ray source (1486.6 eV). For each sample, survey spectra as well as high-resolution core-level windows of carbon 1s, oxygen 1s, nitrogen 1s, sulphur 2p and gold 4f levels were acquired over a spot size of 200 μm and a pass energy of 187.5 eV for spectra and 58.7 eV for windows. Data were processed using the Casa XPS software. The energy calibration is done on CC/CH bonds (1s level at 284.8 eV).

Photo-physical properties. Absorption spectra are recorded on a Specord 205 spectrophotometer (Analytik Jena), fluorescence spectra and 2D maps on a FLSP920 (Edinburgh Instru.). White areas in 2D plots contain no data as fluorescence is recorded from 10 nm above λ_{ex} up to 10 nm before the second harmonic, $2\lambda_{\text{ex}}$. Lifetimes are recorded by time-correlated single photon counting (TCSPC) at 430 nm, with 380-nm pulsed LED for excitation (PLS 370, Picoquant). The AuNC solutions are placed

in 1-cm light-path quartz cells. The 2D maps are built from fluorescence spectra recorded excitation wavelengths from 280 nm to 520 nm with a 5 nm step. Fluorescence decay rates are extracted from a multi-exponential least-square fit of the time evolution of the fluorescence intensity, $I(t)$.

$$I(t) = \sum_{i=1}^n \frac{I_i}{\tau_i} \exp(-t/\tau_i).$$

With I_i the steady-state intensity and τ_i the lifetime of the i^{th} decay. The mean fluorescence lifetime is calculated as:

$$\langle \tau \rangle = \frac{\sum_i \alpha_i \tau_i^2}{\sum_i \alpha_i \tau_i},$$

where α_i is the normalized pre-exponential factor ($I_i = \alpha_i \tau_i$). POPOP dye is used as a lifetime reference ($\tau = 1.35$ ns in ethanol).

Quantum yields are extracted as:

$$\phi = \frac{S}{S_r} \frac{OD_r}{OD} \left(\frac{n}{n_r} \right)^2 \phi_r,$$

where S is the integrated fluorescence intensity, OD is the optical density and n is the refractive index (r index denotes the reference sample). Quantum yields of Rhodamine G ($\Phi = 0.95$ in ethanol) and 9,10-Bis(phenylethynyl)anthracene ($\Phi = 1$ in cyclohexane) are used as references.

The spectrum of the white luminescence is recorded by broadband excitation from a standard fluorescence illuminator with pre-centered liquid light guide (Intensilight C-HGFI, ultrahigh pressure 130 W mercury lamp, Nikon France) and a 350-500 nm bandpass filter. As the excitation and emission range overlap, the normalized lamp spectrum recorded by scattering on a needle is subtracted.

Conflicts of interest

There are no conflicts to declare.

Acknowledgements

The authors thank C. Bernard-Nicod for technical assistance in XPS experiments. This work was funded by the Agence Nationale de la Recherche (ANR, Contracts No. ANR-14-CE08-0004-ARTEMIS and No ANR-16-CE09-0027-HybNaP). This research was partially supported by the project STIM – REI, Contract Number: KK.01.1.1.01.0003, funded by the European Union through the European Regional Development Fund – the Operational Programme Competitiveness and Cohesion 2014-2020 (KK.01.1.1.01) and the CEFIPRA project No 6108-1.

Notes and references

- 1 P. Alivisatos, *Nature Biotechnology*, 2004, **22**, 47–52.
- 2 X. Michalet, *Science*, 2005, **307**, 538–544.
- 3 H.-C. Chang, Y.-F. Chang, N.-C. Fan and J. A. Ho, *ACS Applied Materials & Interfaces*, 2014, **6**, 18824–18831.
- 4 M. Haruta, N. Yamada, T. Kobayashi and S. Iijima, *J. Catalysis*, 1989, **115**, 301–309.
- 5 A. H. Mueller, M. A. Petruska, M. Achermann, D. J. Werder, E. A. Akhador, D. D. Koleske, M. A. Hoffbauer and V. I. Klimov, *Nano Letters*, 2005, **5**, 1039–1044.

- 6 A. M. Derfus, W. C. W. Chan and S. N. Bhatia, *Nano Letters*, 2004, **4**, 11–18.
- 7 M. C. Mancini, B. A. Kairdolf, A. M. Smith and S. Nie, *Journal of the American Chemical Society*, 2008, **130**, 10836–10837.
- 8 R. Hardman, *Environmental Health Perspectives*, 2006, **114**, 165–172.
- 9 C. Eggeling, J. Widengren, R. Rigler and C. A. M. Seidel, *Anal. Chem.*, 1998, **70**, 2651–2659.
- 10 M. Zhu, C. M. Aikens, F. J. Hollander, G. C. Schatz and R. Jin, *Journal of the American Chemical Society*, 2008, **130**, 5883–5885.
- 11 J. M. Forward, D. Bohmann, J. P. Fackler and R. J. Staples, *Inorganic Chemistry*, 1995, **34**, 6330–6336.
- 12 I. Chakraborty and T. Pradeep, *Chemical Reviews*, 2017, **117**, 8208–8271.
- 13 R. Jin, C. Zeng, M. Zhou and Y. Chen, *Chemical Reviews*, 2016, **116**, 10346–10413.
- 14 J. Xie, Y. Zheng and J. Y. Ying, *Journal of the American Chemical Society*, 2009, **131**, 888–889.
- 15 J. Zheng, J. T. Petty and R. M. Dickson, *Journal of the American Chemical Society*, 2003, **125**, 7780–7781.
- 16 J. Zheng, C. Zhang and R. M. Dickson, *Physical Review Letters*, DOI:10.1103/PhysRevLett.93.077402.
- 17 M. A. Habeeb Muhammed, S. Ramesh, S. S. Sinha, S. K. Pal and T. Pradeep, *Nano Research*, 2008, **1**, 333–340.
- 18 H. Qian, Y. Zhu and R. Jin, *ACS Nano*, 2009, **3**, 3795–3803.
- 19 L. Shang, N. Azadfar, F. Stockmar, W. Send, V. Trouillet, M. Bruns, D. Gerthsen and G. U. Nienhaus, *Small*, 2011, **7**, 2614–2620.
- 20 H. Kawasaki, K. Hamaguchi, I. Osaka and R. Arakawa, *Advanced Functional Materials*, 2011, **21**, 3508–3515.
- 21 Y. Bao, H.-C. Yeh, C. Zhong, S. A. Ivanov, J. K. Sharma, M. L. Neidig, D. M. Vu, A. P. Shreve, R. B. Dyer, J. H. Werner and J. S. Martinez, *The Journal of Physical Chemistry C*, 2010, **114**, 15879–15882.
- 22 K. Pyo, V. D. Thanthirige, K. Kwak, P. Pandurangan, G. Ramakrishna and D. Lee, *Journal of the American Chemical Society*, 2015, **137**, 8244–8250.
- 23 X. Kang and M. Zhu, *Chemical Society Reviews*, 2019, **48**, 2422–2457.
- 24 F. Bertorelle, C. Moulin, A. Soleilhac, C. Comby-Zerbino, P. Dugourd, I. Russier-Antoine, P.-F. Brevet and R. Antoine, *ChemPhysChem*, 2018, **19**, 165–168.
- 25 F. Bertorelle, I. Russier-Antoine, N. Calin, C. Comby-Zerbino, A. Bensalah-Ledoux, S. Guy, P. Dugourd, P.-F. Brevet, Ž. Sanader, M. Krstić, V. Bonačić-Koutecký and R. Antoine, *The Journal of Physical Chemistry Letters*, 2017, **8**, 1979–1985.
- 26 C. Lavenn, F. Albrieux, A. Tuel and A. Demessence, *Journal of Colloid and Interface Science*, 2014, **418**, 234–239.
- 27 H. Wei, Z. Wang, L. Yang, S. Tian, C. Hou and Y. Lu, *The Analyst*, 2010, **135**, 1406–1410.
- 28 M. P. Johansson, A. Lechtken, D. Schooss, M. M. Kappes and F. Furche, *Physical Review A*, 2008, **77**, 053202.
- 29 M. P. Johansson, I. Warnke, A. Le and F. Furche, *The Journal of Physical Chemistry C*, 2014, **118**, 29370–29377.
- 30 A. Soleilhac, F. Bertorelle, C. Comby-Zerbino, F. Chirot, N. Calin, P. Dugourd and R. Antoine, *The Journal of Physical Chemistry C*, 2017, **121**, 27733–27740.
- 31 K. L. D. M. Weerawardene, H. Häkkinen and C. M. Aikens, *Annu. Rev. Phys. Chem.*, 2018, **69**, 205–229.
- 32 V. Bonačić-Koutecký and R. Antoine, *Nanoscale*, 2019, **11**, 12436–12448.
- 33 M. Walter, J. Akola, O. Lopez-Acevedo, P. D. Jadzinsky, G. Calero, C. J. Ackerson, R. L. Whetten, H. Gronbeck and H. Häkkinen, *Proceedings of the National Academy of Sciences*, 2008, **105**, 9157–9162.
- 34 Y. Shichibu, Y. Negishi, T. Tsukuda and T. Teranishi, *Journal of the American Chemical Society*, 2005, **127**, 13464–13465.
- 35 C. Comby-Zerbino, X. Dagany, F. Chirot, P. Dugourd and R. Antoine, *Mater. Adv.*, 2021, **2**, 4896–4913.
- 36 C. Truillet, F. Lux, O. Tillement, P. Dugourd and R. Antoine, *Anal. Chem.*, 2013, **85**, 10440–10447.
- 37 J. J. Hagen and C. A. Monnig, *Anal. Chem.*, 1994, **66**, 1877–1883.
- 38 F. Aldeek, M. A. H. Muhammed, G. Palui, N. Zhan and H. Mattoussi, *ACS Nano*, 2013, **7**, 2509–2521.
- 39 J.-H. Jou, Y.-T. Su, S.-H. Liu, Z.-K. He, S. Sahoo, H.-H. Yu, S.-Z. Chen, C.-W. Wang and J.-R. Lee, *J. Mater. Chem. C*, 2016, **4**, 6070–6077.
- 40 S. Muthu, F. J. P. Schuurmans and M. D. Pashley, *IEEE J. Sel. Top. Quantum Electron.*, 2002, **8**, 333–338.
- 41 M. A. Baldo, D. F. O'Brien, Y. You, A. Shoustikov, S. Sibley, M. E. Thompson and S. R. Forrest, *Nature*, 1998, **395**, 151–154.
- 42 N. Thejokalyani and S. J. Dhoble, *Renewable and Sustainable Energy Reviews*, 2014, **32**, 448–467.
- 43 K. Pyo, H. Xu, S. M. Han, S. Saxena, S. Y. Yoon, G. Wiederrecht, G. Ramakrishna and D. Lee, *Small*, 2021, **17**, 2004836.
- 44 A. D. Kurdekar, L. A. Avinash Chunduri, C. S. Manohar, M. K. Haleyurgirisetty, I. K. Hewlett and K. Venkataramaniah, *Science Advances*, 2018, **4**, eaar6280.
- 45 F. Yesilkoy, E. R. Arvelo, Y. Jahani, M. Liu, A. Tittl, V. Cevher, Y. Kivshar and H. Altug, *Nat. Photonics*, 2019, **13**, 390–396.
- 46 B. Musnier, K. D. Wegner, C. Comby-Zerbino, V. Trouillet, M. Jourdan, I. Häusler, R. Antoine, J.-L. Coll, U. Resch-Genger and X. Le Guével, *Nanoscale*, 2019, **11**, 12092–12096.
- 47 D. Shen, M. Henry, V. Trouillet, C. Comby-Zerbino, F. Bertorelle, L. Sancey, R. Antoine, J.-L. Coll, V. Josserand and X. Le Guével, *APL Materials*, 2017, **5**, 053404.

Facile One-Pot Synthesis of White Emitting Gold Nanocluster solutions composed of Red, Green and Blue Emitters

Laureen Moreaud,^a Janak Prasad,^a Serges Mazères,^b Cécile Marcelot,^a Clothilde

Comby-Zerbino,^c Rodolphe Antoine,^c Olivier Heintz^d and Erik Dujardin^{*a}

^a CEMES, CNRS UPR 8011– Université Toulouse III P. Sabatier, 29 rue J. Marvig, 31055 Toulouse, France. Email: dujardin@cemes.fr

^b IPBS, CNRS UMR 5089 – Université Toulouse III P. Sabatier, 205 route de Narbonne, 31077 Toulouse, France.

^c ILM, CNRS UMR 5306 - Université C. Bernard Lyon 1, 69100 Villeurbanne, France.

^d ICB, CNRS UMR 6303 – Université de Bourgogne Franche-Comté, 9 rue A. Savary, 21078 Dijon, France

* Corresponding author: dujardin@cemes.fr

Electronic Supporting Information

Table of contents

| | |
|--|-------|
| 1. Control experiments on the fluorescence emission (Fig. S1) | p. 2 |
| 2. UV-visible absorption spectrum (Figs. S2) | p. 3 |
| 3. Repeatability tests (Figs. S3) | p. 4 |
| 4. Effect of thiopegylation on photophysical properties (Figs. S4) | p. 5 |
| 5. Au cluster sizes calculated from the Jellium model (Table S5) | p. 6 |
| 6. XPS analysis of functionalized AuNC (Fig. S6) | p. 7 |
| 7. ESI-MS of thiopegylated AuNCs (Figs. S7, S8) | p. 8 |
| 8. HRTEM study of AuNCs (Figs. S9, S10) | p. 10 |
| 9. AFM topography of AuNCs (Fig. S11) | p. 12 |
| 10. Fluorescence lifetime measurements of thiopegylated AuNCs (Fig. S12) | p. 13 |
| 11. Analysis of quantum yields reported in the literature for water-soluble AuNC (Fig. S13) | p. 14 |
| 12. Quantum yield of thiopegylated AuNC (Table S14) | p. 15 |
| 13. References | p. 16 |

1 - Control experiments on the fluorescence emission

Pure EG is crucial in the formation of bright emitting AuNCs. A slight dilution of EG with water leads to an immediate reduction of the mixture fluorescence, irrespective of the excitation energy, until it completely disappears and only larger plasmonic non fluorescent gold nanoparticles are obtained instead of fluorescent AuNCs (Figs. S1a-c). In standard fluorescence spectroscopy experiments, the presence of larger gold nanoparticles is revealed by the second harmonic peak of the excitation corresponding to the diffusion of the excitation light by the metallic surface. These peaks are the only ones present in fluorescence spectra from 10 nm gold nanoparticles stabilized with citrate (Fig S1d), are clearly observed in 95% EG solutions (Fig S1b) or in the absence of EG (Fig S1b) but are not seen in spectra of 100% EG samples (Fig S1a).

The observed fluorescence could be produced by the adducts of other reagents used in our protocol. We have therefore conducted several control experiments by following the same protocol in 100% EG as the generic synthesis but omitting one component. When the aniline is not added, no fluorescence signal is obtained (Fig. S1e). In the absence of gold precursor, a small emission peak centered at 340 nm is recorded that is absent of all AuNC fluorescence spectra (Fig. S1f). The origin of this fluorescence was not identified.

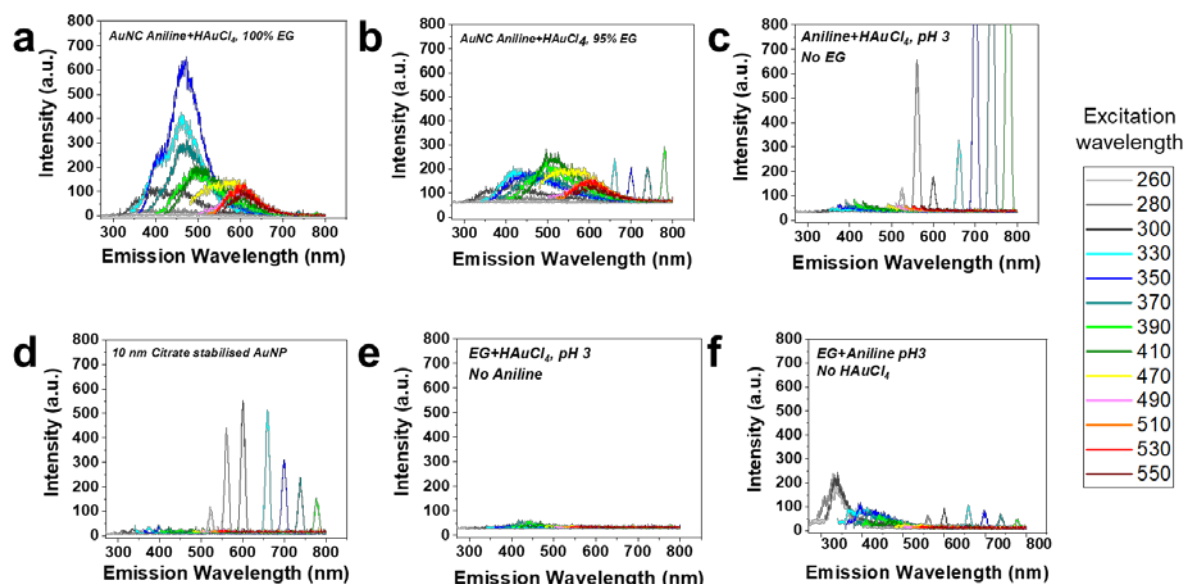


Figure S1: Fluorescence spectra of (a) as-synthesized AuNCs obtained by the standard aniline protocol; (b) a solution produced in 95% EG; (c) a solution produced in the absence of EG. (d) Fluorescence spectra of a solution of 10 nm citrate stabilized AuNPs that exhibit only excitation harmonic scattering. (e,f) Fluorescence spectra of control solutions obtained by the generic protocol without adding (e) aniline or (f) HAuCl₄. All panels follow the same color coding of the excitation wavelength shown on the right.

2 - UV-visible absorption spectrum

The UV-vis absorbance spectra of as-synthesized as well as functionalized and dialyzed samples produced with aniline or indole are shown in Figure S2. The decrease of absorbance after the functionalization is attributed to the dilution during the dialysis step.

The peaks with a spectral broadening of the absorption spectrum due to a molecule-like HOMO-LUMO transition is characteristic of ultra-small metallic particles. Only the as-synthesized indole-based solution (Fig. S2b, black curve) shows a peak that could indicate the presence of small plasmonics particles larger than 3 nm diameter. Even though centrifugation of the as-synthesized suspensions reduces the presence of large nanoparticles, EG is viscous and complicates the full removal of the plasmonics colloids. In contrast, the spectra after functionalization and dialysis (red curves) do not show any plasmon peak, indicating that the particles are smaller than 3 nm. The transfer protocol into water described in Experimental Section thus leads to Au nanoclusters solutions free of plasmonic nanocrystals.

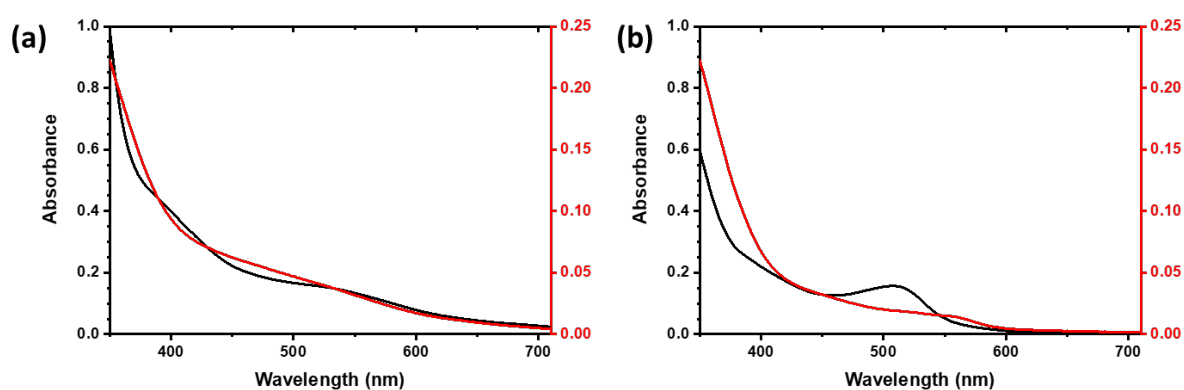


Figure S2. UV-vis absorption spectrum after centrifugation of as-synthesized solution (in black) and functionalized then dialyzed solution (in red) of: (a) aniline-reduced sample and (b) indole-reduced sample.

3. Repeatability of the one-pot AuNC synthesis

The 2D fluorescence maps of several repeats of our one-step synthesis yield highly reproducible positions of the high-intensity areas for both aniline (AuNCa) and indole (AuNCi) protocols even before any post-synthetic processing (centrifugation, dialysis or functionalization).

Figure S3 shows two pairs of 2D fluorescence maps corresponding to two different batches (a,c and b,d) for both protocols, AuNCa (a,b) and AuNCi (c, d). The same excitation / emission areas (pinpointed by sets of black crosses placed at the same coordinates for both batches) are observed with very minor relative intensity changes.

Note that the instrumental noise is higher on the second batch (Figs. S3b, d) due to a lower intensity of the solution emission. In these low concentration conditions, artifacts due to the Raman peaks of the water are visible. Their spectral position varies linearly with the excitation wavelength and so are visible on the 2D map as diagonal straight lines. These artifacts are often used to calibrate fluorescence spectrometers. The presence of water in the second synthesis can be explained by the hygroscopic character of EG. In this particular synthesis, EG with measurable traces of absorbed water was used.

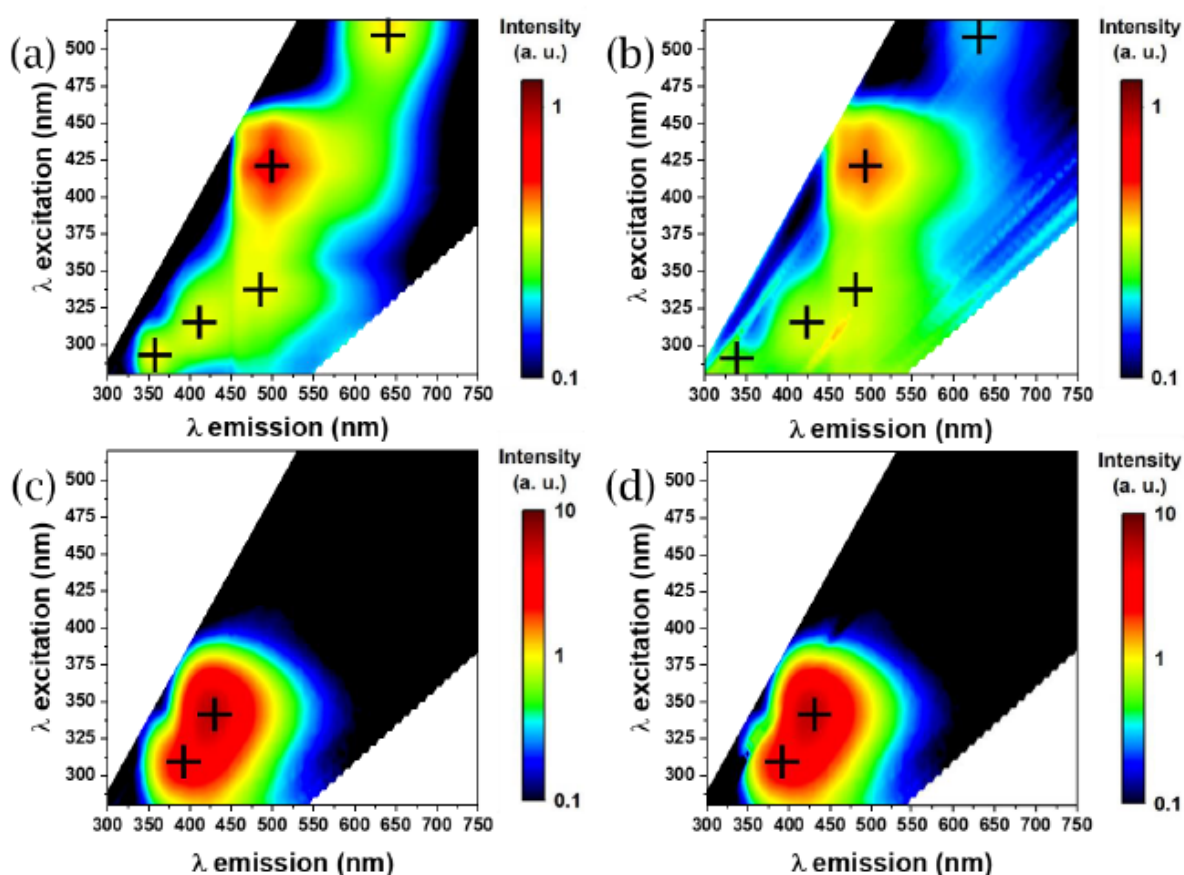


Figure S3 Representative 2D maps of room temperature fluorescence intensity of (a-b) AuNCa and (c-d) AuNCi clusters as a function of emission (λ_{em}) and excitation (λ_{ex}) wavelengths from two different batches. Black crosses in (a) and (b), respectively (c) and (d), are placed at the same (λ_{em} , λ_{ex}) coordinates. The white areas of the 2D plots contain no data, as fluorescence is recorded from 10 nm above λ_{ex} to 10 nm before the second harmonic, $2\lambda_{ex}$.

4. Effect of thiopegylation on photophysical properties

The functionalization of the clusters by water-soluble thiopegylated ligands bearing any of the three considered terminal groups only marginally impacts the spectral positions of the fluorescence features. Figure S4 gathers the 2D fluorescence maps of AuNCa (a,c,e) and AuNCi (b, d, f) after functionalization with (a,b) short PEG amine **1**, (c, d) short PEG carboxylate **2** and (e, f) long PEG biotin **4**. The black cross markers in Fig. S4 are placed in the same $(\lambda_{em}, \lambda_{ex})$ coordinates as in figure S3. In all cases, the luminescence patterns coincide with those of as-synthesized AuNC, irrespective of the ligand. One can note the further blue shift from $\lambda_{em} = 352$ nm to $\lambda_{em} = 310$ -330 nm of the violet emitters in thiopegylated AuNCa.

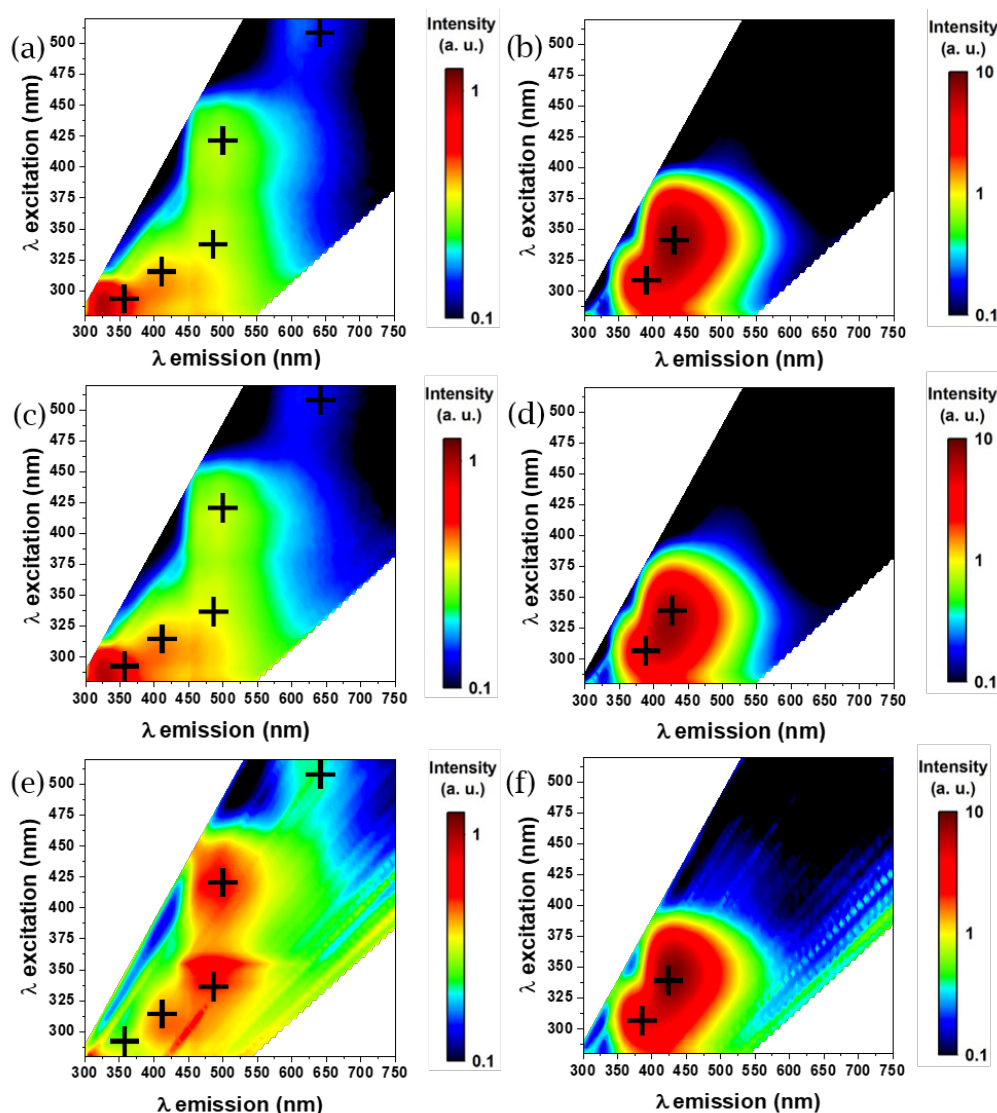


Figure S4: 2D maps of room temperature fluorescence intensity of thiopegylated AuNC (a) 1a, (b) 1i, (c) 2a, (d) 2i, (e) 4a and (f) 4i in water as a function of emission (λ_{em}) and excitation (λ_{ex}) wavelengths.

However, the main impact of the functionalization is a redistribution of the relative intensity between the different emitters for the aniline AuNCa capped with short (PEG₁₂) ligands 1a (Fig. S4a) and 2a (Fig. S4c). The strongest emission is no longer the green one ($\lambda_{ex} = 425$ nm; $\lambda_{em} = 500$ nm) but violet ($\lambda_{ex} = 290$ nm; $\lambda_{em} = 325$ nm).

This is much less marked in biotinylated AuNC 4a (Fig. S4e), for which the relative intensities match those of as-synthesised clusters. Remarkably, all indole AuNCi show absolutely no spectral nor intensity change upon thiopegylation and transfer into water

5. Au cluster size calculated from the Jellium model

The fluorescence intensity 2D maps shown in Figure 1 display high intensity spots that are associated with AuNCs. The emission wavelength of the maximal intensity, λ_{em}^{max} , as well as the extremal wavelengths corresponding to 80% of this maximum are shown for both aniline and indole AuNCs in the first column of Table S5. The second column converts λ_{em}^{max} in energy units.

In the last column, the Jellium model is used to estimate, with an interval, the number of Au atoms of an AuNCs emitting at λ_{em}^{max} (E_f is the Fermi energy of bulk gold).

| Type de Clusters | λ_{em}^{max} (80% range) (nm) | E (eV) | $n = \left(\frac{E_f}{E}\right)^3$ |
|------------------|--|--------|------------------------------------|
| Indole | 400 (375-430) | 3,10 | 5 (4-7) |
| | 425 (400-450) | 2,92 | 7 (5-8) |
| Aniline | 410 (350-450) | 3,02 | 6 (4-8) |
| | 500 (460-540) | 2,48 | 11 (8-13) |
| | 640 (600-670) | 1,94 | 22 (18-26) |

Table S5: AuNC size estimated from the fluorescence 2D maps using the Jellium model for both aniline and indole samples.

6. XPS analysis of functionalized AuNC

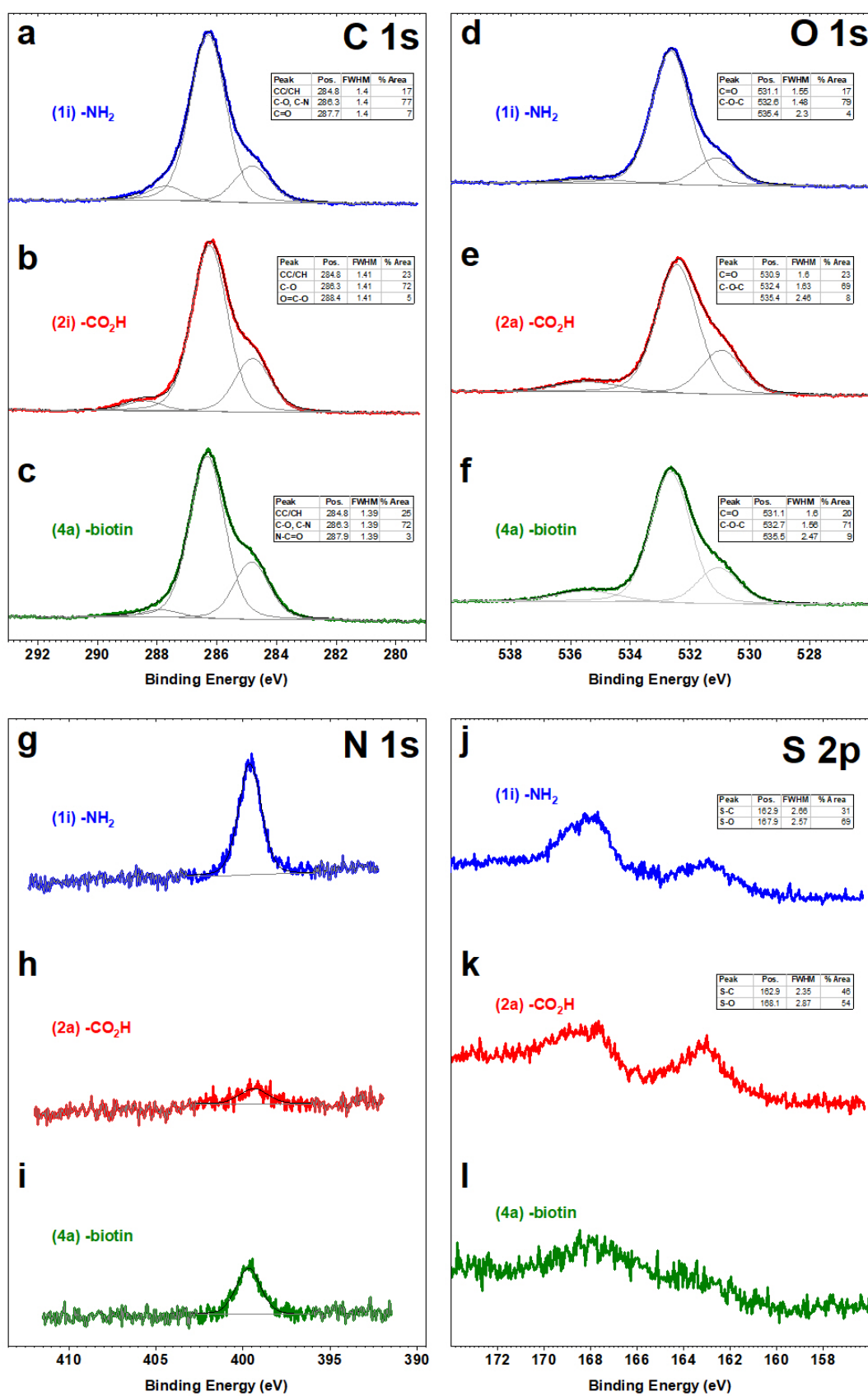


Figure S6: XPS spectra of -NH₂ (blue), -CO₂H (red) and -biotin (green) thiopegylated AuNC. (a-c) C1s level. (d-f) O1s level. (g-i) N1s level. (j-l) S2p level.

7. ElectroSpray Ionization Mass Spectrometry of thiopegylated AuNCs

ESI-MS spectra of AuNC with PEG₁₂ containing ligands.

Figure 3, in the main text, presents the negative mode mass-to-charge ESI-MS spectra for (2a) and (2i) AuNCs exchanged with HS-PEG₁₂-COOH.

Three different cores from aniline-reduced clusters (2a) have been identified consistently with photophysical and XPS data: Au₄, Au₇ and Au₁₀. The dominant peaks numbered from 1 to 7 were associated with: (1, m/z = 2906) [Au₇(S-PEG₁₂-CO₂H)₇]²⁻, (2, m/z = 3222) [Au₇(S-PEG₁₂-CO₂H)₈]²⁻, (3, m/z = 4154) [Au₁₀(S-PEG₁₂-CO₂H)₁₀]²⁻.

Polymerized PEG₁₂-CO₂H fragments are also observed: (i) trimer (m/z = 1902), (ii) tetramer (m/z = 2535), (iii) pentamer (m/z = 3169)

Similarly, for indole-reduced clusters (2i), the dominant peaks, numbered from 1 to 8, suggest the presence of Au₁₀, Au₁₁ and Au₁₂ clusters: (1, m/z = 4168) [Au₁₀(S-PEG₁₂-CO₂H)₁₀]²⁻, (2, m/z = 4471) [Au₁₀(S-PEG₁₂-CO₂H)₁₁]²⁻, (3, m/z = 4569) [Au₁₁(S-PEG₁₂-CO₂H)₁₁]²⁻, (4, m/z = 4788) [Au₁₀(S-PEG₁₂-CO₂H)₁₂]²⁻, (5, m/z = 4885) [Au₁₁(S-PEG₁₂-CO₂H)₁₂]²⁻, (6, m/z = 4984) [Au₁₂(S-PEG₁₂-CO₂H)₁₂]²⁻, (7, m/z = 5304) [Au₁₂(S-PEG₁₂-CO₂H)₁₃]²⁻, (8, m/z = 5619) [Au₁₂(S-PEG₁₂-CO₂H)₁₄]²⁻

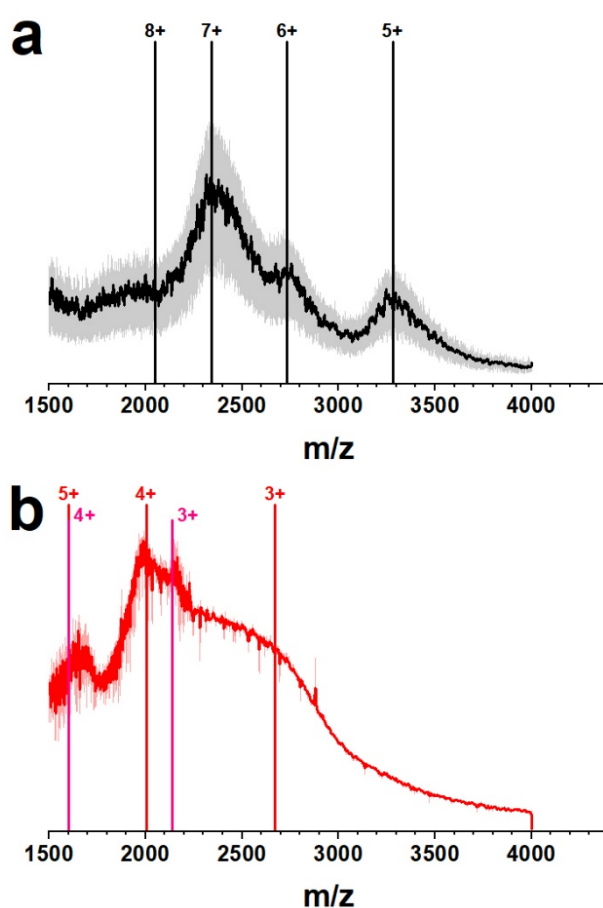


Figure S7: Positive mode mass-to-charge ESI-MS spectra for (1a) and (1i) AuNCs respectively exchanged with HS-PEG₁₂-NH₂ from aniline (panel a) and indole (panel b) gold clusters. A broad distribution of charge states is observed in both cases that can be assigned to Au₂₅(S-PEG₁₂-NH₂)₁₉ in (1a), as shown by the 5+ to 8+ markers in panel a, and to Au₁₀(S-PEG₁₂-NH₂)₁₀ with Au₈(S-PEG₁₂-NH₂)₈ in (1i) as indicated by the 3+ to 5+ red markers and 3+ to 4+ pink markers respectively in panel b. In both panels, smoothed data are shown in dark color on top of the fainter raw data.

The positive mode spectra of amine-stabilized AuNC shown in Figure S7 comprise a significant contribution of the PEG fragments, in particular in the 500 < m/z < 1500 region, therefore preventing to assert the presence of very small AuNC. Yet, in the 1500-4000 region, one can observe peaks that can

be matched to $\text{Au}_{25}(\text{S-PEG}_{12}\text{-NH}_2)_{19}$ with average mass of 16.4 kDa in (1a) and to $\text{Au}_{10}(\text{S-PEG}_{12}\text{-NH}_2)_{10}$ with average mass 8 kDa, plus $\text{Au}_8(\text{S-PEG}_{12}\text{-NH}_2)_8$ with average mass of 6.4 kDa in (1i).

ESI-MS spectra of AuNC with PEG₇₀ containing ligands.

The biotinylated AuNC 4a/4i were functionalized with a high molecular weight PEG spacer (~3 000 Da) in order to ensure their long term stability in aqueous solution. Figure S8 below shows the ESI-MS spectra in positive mode and its deconvolution using a multiplicative correlation algorithm.

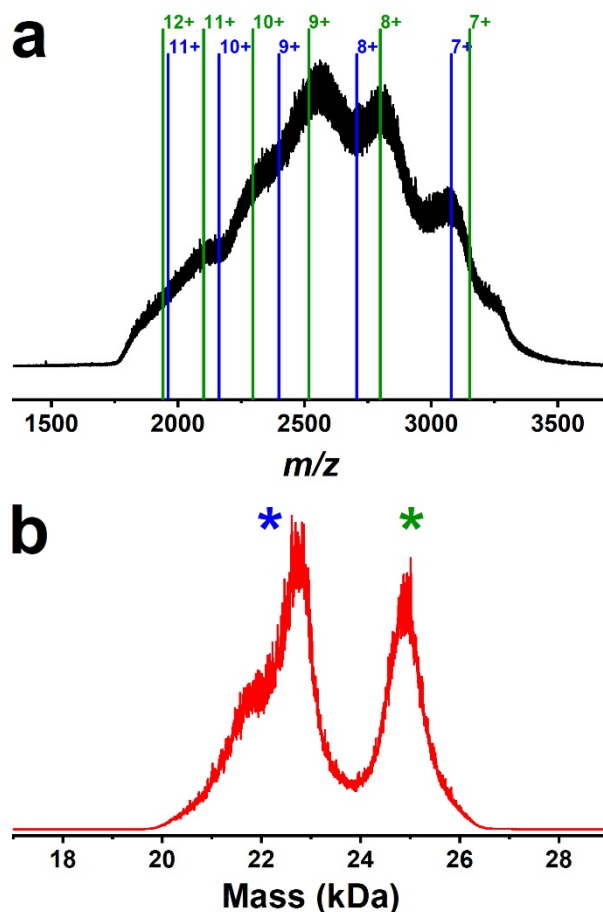


Figure S8: (a) Mass-to-charge spectra of 4a AuNCs stabilized with long biotinylated thioPEG ligands recorded in positive mode. Charge states for $\text{Au}_6(\text{S-PEG}_{70}\text{-Biotin})_6$ and $\text{Au}_7(\text{S-PEG}_{70}\text{-Biotin})_7$ are shown in blue and green lines respectively. (b) ESI-MS spectrum deconvoluted with a multiplicative correlation algorithm and showing two peaks compatible with Au_6 (blue marker) and Au_7 (green marker) AuNCs.

Note on MALDI-MS measurements

We also made attempts to measure the mass of the as-prepared Au NCs. For this purpose, we performed MALDI-MS measurements using a Voyager-DE PRO Biospectrometry Workstation from Applied Biosystems. A pulsed nitrogen laser of 337 nm was used for ionizing the sample, and alpha-Cyano-4-hydroxycinnamic acid was used as the matrix. The MALDI-MS show no information regarding intact nanoclusters. Only fragments or PEG envelopes were measured by MALDI-MS (data not shown).

8. HRTEM study of AuNCs

The direct size, morphology and structure characterization of sub-3 nm AuNCs remains challenging. Besides electrospray mass spectrometry (ESI-MS) and X-ray photoelectrons spectroscopy (XPS), the pristine AuNCs are characterized by high-resolution transmission electron microscope (HRTEM) as shown in Figures S9 and S10.

HRTEM images of non-thiolated AuNCs show no sign of aggregation, a homogeneous shape and a lognormal size distribution with an overall mean and standard deviation of the gold core diameter of 2.9 ± 1.6 nm and 2.4 ± 0.7 nm for aniline and indole reduced clusters respectively (Figs. S9a and S9b). These distributions underestimate the smallest clusters that have an extremely weak TEM contrast since the most stable form of AuNC with less than 13 atoms is considered to be flat oligomeric structures.¹⁻³ This suggests the coexistence of clusters with different optical properties. Clusters with diameters larger than 2.2 nm are considered poor emitters while clusters smaller than 2.2 nm exhibit linear and non-linear luminescence⁴. Since our samples precisely overlap this boundary, as confirmed by atomic force microscopy measurements yielding a height of 1.7 ± 0.7 nm (ESI Fig. S11), we have further examined the AuNCs morphology. Essentially, four different structures of AuNCs are observed in both aniline- and indole-reduced samples and show a gradual shift in size distribution (Figs. S9c-f). A lattice parameter of 2.35 Å could be observed for all shapes, that corresponds to the (111) plane family of a gold face-centered cubic crystal packing (See also Fig. S10).

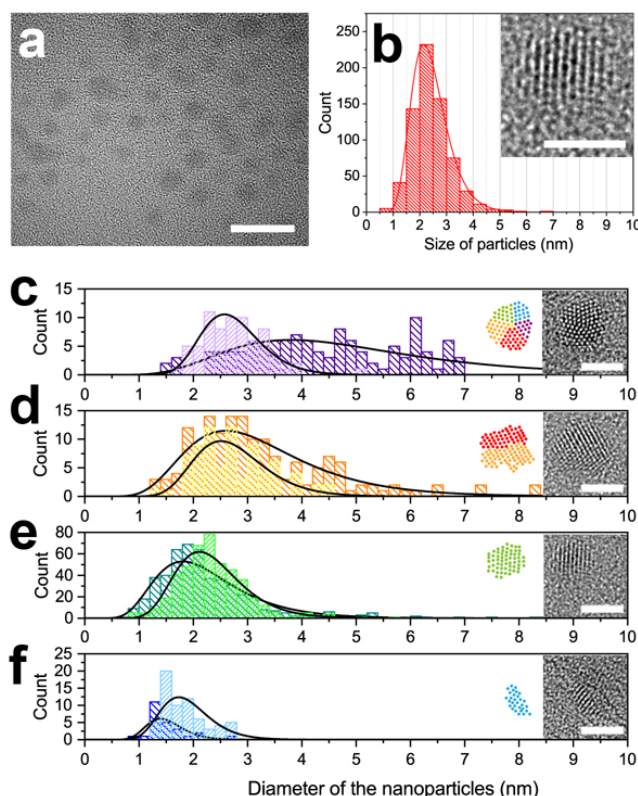


Figure S9. (a) Typical HRTEM image of as-synthesized indole AuNCs. (b) Size distribution of the indole AuNCs. The mean size is 2.4 ± 0.7 nm. Inset: close-up TEM image displaying the crystal lattice of one indole AuNC. (c-f) Size histograms of indole (lighter colors) and aniline (darker colors) AuNCs sorted into shape classes illustrated by the TEM image and colored sketch insets: (c) pentatwin, (d) single twin, (e) isotropic single crystal, (f) oblong single crystals. Scale bars 2 nm. Black lines are lognormal fits.

The larger AuNCs (5.0 ± 2.2 nm with aniline and 2.7 ± 0.6 nm with indole) are composed of 5 twins but represent only 14-16%. The second larger structures (3.3 ± 1.3 nm with aniline and 2.7 ± 0.7 nm with indole) are single twinned and amount to 11-20%. The two smallest sub-populations appear single crystalline but present two different shapes. The isotropic structures represent 61-66% (2.27 ± 0.91 nm with aniline and 2.36 ± 0.65 nm with indole). The oblong AuNCs amounts to 3-9% and their longer and

shorter axes are 1.51 ± 0.35 nm and 1.07 ± 0.11 nm with aniline and 1.90 ± 0.47 nm and 1.04 ± 0.16 nm with indole respectively. These smallest and lower contrast nanostructures could be commensurate with Au₁₀ to Au₁₃ that sit at the onset between 2D and 3D morphologies, have a typical size of ca. 1.1-1.2 nm and show oblong anisotropy in the more stable 2D forms^{2,3}.

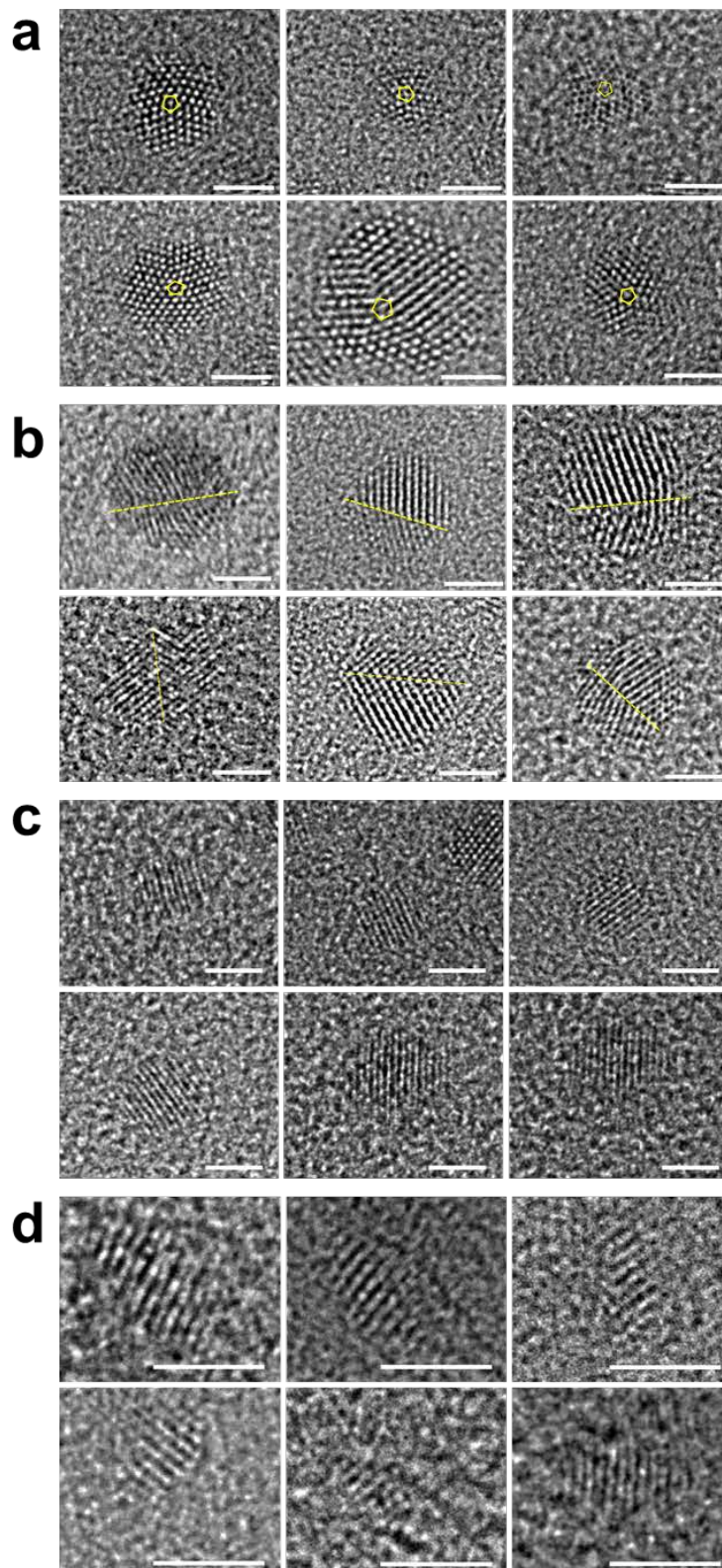


Figure S10: High resolution TEM micrographs of as-synthesized (a) pentatwinned, (b) single twinned, (c) isotropic single crystalline and (d) oblong single crystalline AuNCs. Scale bars are 2 nm.

9. AFM topography of AuNCs

The AuNCs were dispersed on a freshly cleaved mica substrate by drop-casting and drying a microdroplet. AFM images were acquired on a Bruker DI 3000 microscope operated in intermittent mode using OTESPA silicon tips (Bruker, ca. 300 kHz resonance). A typical AFM image of AuNCs is shown in Fig. S3a and is compared with an image of a pristine mica surface in Fig. S3 b. Height profiles and height histograms of both samples are plotted in Figures S3 c,d and S3e,f respectively.

The clear presence of dispersed dots with lateral size of ca. 20 nm limited by the tip convolution and height of a few Angstroms is consistent with the TEM images and the size histograms shown in Fig. S9 and can be ascribed to AuNCs. If one considers the AFM height as the relevant size gauge the AuNC apparent size, the average height is $1.7 \text{ nm} \pm 0.7 \text{ nm}$. This suggests the presence of sub-3 nm clusters.

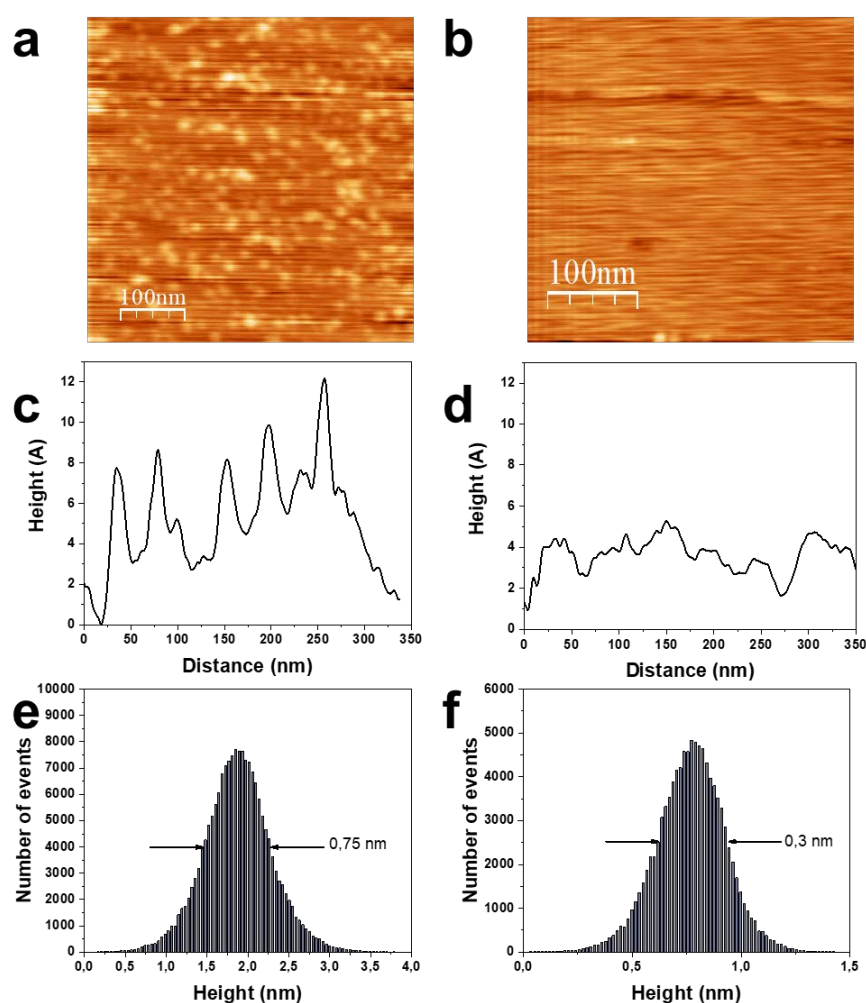


Figure S11: (a-b) AFM topography images of AuNCs on mica and freshly cleaved mica. (c-d) Height profiles of the surface of AuNCs on mica and mica alone. (e-f) Histograms of the height of the samples: $1.7 \text{ nm} \pm 0.7 \text{ nm}$ for AuNCs on mica and $0.7 \text{ nm} \pm 0.3 \text{ nm}$ on cleaved mica.

10. Fluorescence lifetime measurements of thiopegylated AuNCs

The fluorescence lifetime measurements for biotin-functionalized aniline (4a) and indole (4i) AuNC shown in Figure S5 do not show any difference with the data for as-synthesized AuNC shown in Figure 4. The lifetime for aniline AuNC 4a is fitted with three decreasing exponentials at 0.50 ns (89%), 5 ns (10%), and 90 ns (1%). The lifetime of indole AuNC 4i is fitted with two exponentials at 0.50 ns (50%) and 8 ns (50%). The exactly matching fit parameters further confirms that the introduction of thiopegylated ligand has virtually no effect on the photophysical properties of the AuNC. It strongly suggests that the HS-PEG_n-R ligand exchange does not affect the emitting center structure and immediate environment.

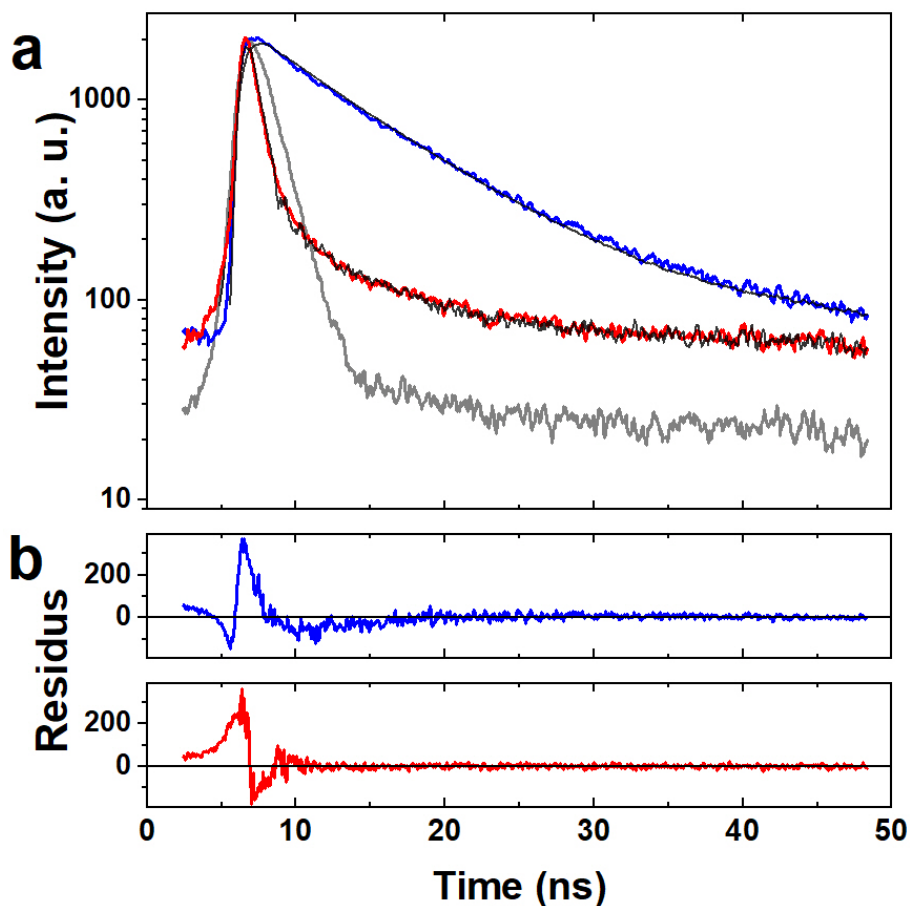


Figure S12. (a) Fluorescence lifetime measurements and (b) fit residues of biotin-functionalized aniline (4a, red) and indole (4i, blue) AuNCs. In (a), fits are in black and the POPOP reference used is in grey.

11. Analysis of quantum yields reported in the literature for water-soluble AuNC

Figure S13 gathers quantum yields of AuNC in water, as reported in the literature by many groups, as a function of the cluster size. This size is either known from available MS experiments or DFT modelization (blue squares) or inferred from available fluorescence spectra using the Jellium model (black squares). Two distinct trends are observed as clearly pointed out by the shaded zones.

Grey zone: AuNC stabilized with small molecular ligands tend to show quantum yield around 5-10% irrespective of their size between 5 and 40 Au atoms.⁵⁻¹⁵

Blue zone: Au NC stabilized by large or polymeric ligands such as PAMAM dendrimers,^{16,17} PEG_n with n=550 or 750,¹¹ or cellulose¹⁸ show a higher quantum yield (10-15%) that drastically increases up to 70% as the AuNC size decreases down to 5 atoms.

The reason invoked for this marked increase of the quantum yield is the presence of a thick or rigid shell around the fluorescent gold core that stiffens the gold shell surface and alters directly the luminescence of the triplet state.¹⁹

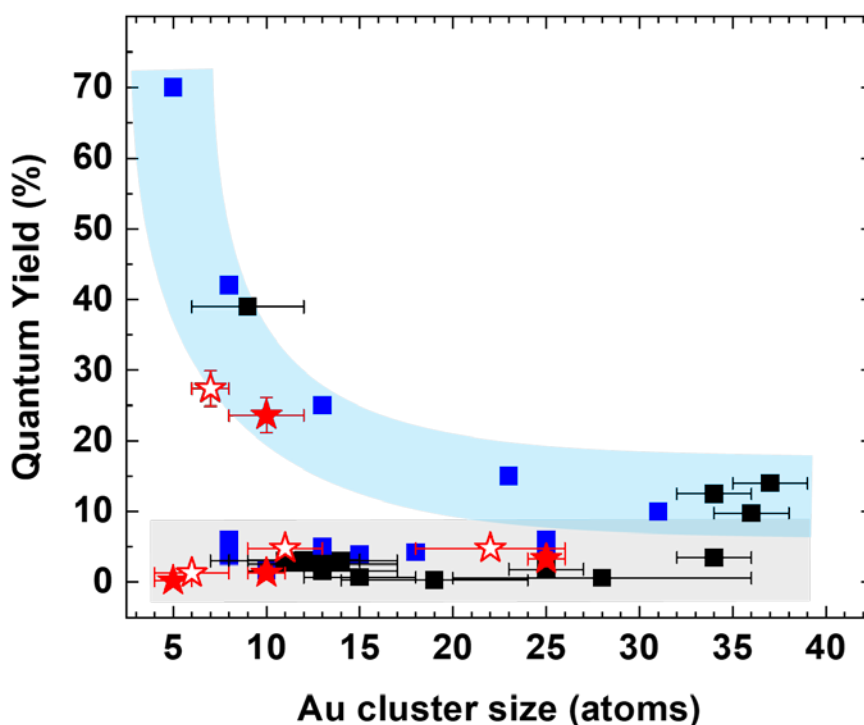


Figure S13. Quantum yields of AuNC reported in the literature (black and blue squares) as a function of cluster size as measured by MS or fixed in DFT models (blue squares) or inferred from luminescence spectra by the Jellium model (black squares). Data reported in this work are inserted as red stars with full symbols when the size is determined by MS (for functionalized AuNC in water) and empty symbols when it is inferred from the Jellium model (for as-synthesized AuNC in EG). Blue and grey shaded zones are only guides for the eye.

When the data reported in this work are added to Figure S13 (red stars), one observes that the green and red emitting AuNC fit into the grey zone as most clusters stabilized with small ligands while the violet/blue emitting AuNC that exhibit a 27% quantum yield reach the blue zone even though the ligand used are much smaller (the larger ones have a PEG₇₀ spacer). Note that empty red stars correspond to as-synthesized AuNC in ethylene glycol while full red stars indicate functionalized AuNC in water as the literature data.

12. Quantum yield of thiopegylated AuNC

| AuNC type | λ_{ex} (nm) | QY (in EG) | AuNC type | QY (in H ₂ O) |
|-----------|---------------------|------------------|-----------|--------------------------|
| AuNCa | 317 | 1.3% \pm 0.5% | 4a | 0.2% \pm 0.5% |
| AuNCa | 395 | 4.8% \pm 0.5% | 4a | 1.3% \pm 1.0% |
| AuNCa | 530 | 4.8% \pm 0.5% | 4a | 3.3% \pm 1.0% |
| AuNCi | 317 | 27.4% \pm 2.5% | 4i | 23.6% \pm 2.5% |

Table S14: Quantum yield (QY) values measured for as-synthesized AuNC_a and AuNC_i clusters in ethylene glycol and for thiopegylated AuNC 4a and 4i in water.

13. References

- 1 A. Soleilhac, F. Bertorelle, C. Comby-Zerbino, F. Chirot, N. Calin, P. Dugourd and R. Antoine, *J. Phys. Chem. C*, 2017, **121**, 27733–27740.
- 2 M. P. Johansson, A. Lechtken, D. Schooss, M. M. Kappes and F. Furche, *Phys. Rev. A*, 2008, **77**, 053202.
- 3 M. P. Johansson, I. Warnke, A. Le and F. Furche, *J. Phys. Chem. C*, 2014, **118**, 29370–29377.
- 4 S. H. Yau, O. Varnavski and T. Goodson, *Acc. Chem. Res.*, 2013, **46**, 1506–1516.
- 5 J. Xie, Y. Zheng and J. Y. Ying, *J. Am. Chem. Soc.*, 2009, **131**, 888–889.
- 6 C.-A. J. Lin, T.-Y. Yang, C.-H. Lee, S. H. Huang, R. A. Sperling, M. Zanella, J. K. Li, J.-L. Shen, H.-H. Wang, H.-I. Yeh, W. J. Parak and W. H. Chang, *ACS Nano*, 2009, **3**, 395–401.
- 7 Y. Bao, H.-C. Yeh, C. Zhong, S. A. Ivanov, J. K. Sharma, M. L. Neidig, D. M. Vu, A. P. Shreve, R. B. Dyer, J. H. Werner and J. S. Martinez, *J. Phys. Chem. C*, 2010, **114**, 15879–15882.
- 8 X. Le Guével, B. Hötzer, G. Jung, K. Hollemeyer, V. Trouillet and M. Schneider, *J. Phys. Chem. C*, 2011, **115**, 10955–10963.
- 9 L. Shang, N. Azadfar, F. Stockmar, W. Send, V. Trouillet, M. Bruns, D. Gerthsen and G. U. Nienhaus, *Small*, 2011, **7**, 2614–2620.
- 10 H. Kawasaki, K. Hamaguchi, I. Osaka and R. Arakawa, *Adv. Funct. Mater.*, 2011, **21**, 3508–3515.
- 11 F. Aldeek, M. A. H. Muhammed, G. Palui, N. Zhan and H. Mattoussi, *ACS Nano*, 2013, **7**, 2509–2521.
- 12 K. G. Stampelcoskie and P. V. Kamat, *J. Am. Chem. Soc.*, 2014, **136**, 11093–11099.
- 13 P.-C. Chen, A. P. Periasamy, S. G. Harroun, W.-P. Wu and H.-T. Chang, *Coord. Chem. Rev.*, 2016, **320–321**, 129–138.
- 14 S. Zhou, Y. Duan, F. Wang and C. Wang, *Nanoscale*, 2017, **9**, 4981–4988.
- 15 X. Jiang, X. Wang, C. Yao, S. Zhu, L. Liu, R. Liu and L. Li, *J. Phys. Chem. Lett.*, 2019, **10**, 5237–5243.
- 16 J. Zheng, J. T. Petty and R. M. Dickson, *J. Am. Chem. Soc.*, 2003, **125**, 7780–7781.
- 17 J. Zheng, C. Zhang and R. M. Dickson, *Phys. Rev. Lett.*, 2004, **93**, 077402.
- 18 S. K. Kailasa, M. R. Kateshiya and N. I. Malek, *J. Mol. Liq.*, 2020, **319**, 114305.
- 19 K. Pyo, V. D. Thanthirige, K. Kwak, P. Pandurangan, G. Ramakrishna and D. Lee, *J. Am. Chem. Soc.*, 2015, **137**, 8244–8250.